JOURNAL OF MATERIALS SCIENCE 16 (1981) 1391–1401

Microstructure and superconductivity in annealed Cu–Nb–(Ti, Zr, Hf) ternary amorphous alloys obtained by liquid quenching

AKIHISA INOUE, C. SURYANARAYANA*,
TSUYOSHI MASUMOTO
The Research Institute for Iron, Steel and Other Metals, Tokohu University, Sendai 980, Japan

Melt-quenched Cu–Nb–(Ti, Zr, Hf) ternary alloys have been found to be amorphous possessing high strength and good bend ductility. The niobium content in the amorphous alloys was limited to less than 35 at % and the titanium, zirconium or hafnium contents from 25 to 50 at %. The $Cu_{40}Nb_{30}(Ti, Hf)_{30}$ alloys showed a superconducting transition above the liquid helium temperature (4.2 K) after annealing at appropriate temperatures. The highest transition temperatures attained were 5.6 K for the $Cu_{40}Nb_{30}Ti_{30}$ alloy annealed for 1 h at 873 K and 8.4 K for the $Cu_{40}Nb_{30}Hf_{30}$ alloy annealed for 1 h at 1073 K. In addition, these alloys exhibited upper critical magnetic fields of 1.8 to 2.3×10^6 A m^{-1} at 4.2 K and critical current densities of 2×10^3 to 1×10^4 A cm^{-2} at zero applied field and 4.2 K. Since the structure of the superconducting samples consisted of ordered phases based on a b c c lattice with a lattice parameter of 0.31 nm, it was concluded that the superconductivity in the $Cu_{40}Nb_{30}Ti_{30}$ and $Cu_{40}Nb_{30}Hf_{30}$ alloys was due to the precipitation of the metastable ordered b c c phases.

1. Introduction

A superconducting material possessing a high critical temperature (T_c) as well as good mechanical properties is desirable from the applications point of view. Since liquid quenching can often produce new metastable phases and these phases generally have superior properties compared with their crystalline counterparts, great interest has been focussed on the study of metastable superconducting materials and the existing data on these metastable superconductors have been extensively reviewed recently [1–3]. The formation of amorphous phases in refractory metal (Ti, Zr, Hf, V, Nb, Ta, Cr, Mo or W)-based alloy systems by melt quenching and their superconducting properties have been investigated and it is reported that the Ti-, Nb-, Mo- and W-based amorphous alloys exhibit superconductivity above the liquid helium temperature [4–15]. However, continuous ribbons of these superconducting alloys were produced under a protective argon atmosphere only when a single-roller quenching apparatus adapted to a levitation furnace described by Masumoto *et al.* [4] was used. If superconducting alloys can be found with melting points low enough to produce continuous tapes using single- or twin-roller quenching apparatus adapted to an induction furnace (a well developed technique) it is expected that amorphous superconductors can readily be obtained without much labour or many elaborate steps. From this point of view, the formation of amorphous alloys with superconductivity has been investigated by conventional melt spinning and it was found that the Cu–Nb–Ti and Cu–Nb–Hf ternary alloys which crystallized from the amorphous state exhibited superconductivity in a limited range of annealing temperatures [11]. The aim of the present paper is to present the details of the composition range for the formation of the amorphous phase in the Cu–Nb–Ti, Cu–Nb–Zr

*Present address: Department of Metallurgical Engineering, Banaras Hindu University, Varanasi-211005, India.

0022–2461/81/051391–11$03.10/0

and Cu–Nb–Hf systems, the crystallization behaviour of the amorphous alloys and the superconducting properties on crystallization of the amorphous alloys.

2. Experimental details

Mixtures of 99.99 wt% pure copper, 99.5 wt% pure niobium, 99.5 wt% pure titanium, 99.6 wt% pure zirconium or 98 wt% pure hafnium were melted in an arc furnace on a water-cooled copper hearth with an unconsumable tungsten electrode. The melting was accomplished in a purified and gettered argon atmosphere at a pressure of about 8×10^4 Pa. The weight of the mixture melted in one run was about 30 to 35 g. The ingots were repeatedly turned over and remelted to insure homogeneity of composition. Weight loss after melting was typically less than 15 mg and the compositions reported are the nominal ones.

Continuous ribbon specimens of about 1 to 2 mm width and 0.02 to 0.03 mm thickness were prepared from these mixed alloys using a conventional single-roller-type quenching apparatus adapted to an induction furnace. Typically, the amount of alloy melted in one run was about 3 g and the rotation speed of the copper roller (20 cm in diameter) was about 6000 rpm.

Identification of the as-quenched phases was made by conventional X-ray diffraction and transmission electron microscope (TEM) methods. The ribbons were classified as amorphous when the X-ray intensity as a function of the diffraction angle showed a typical liquid-like structure. The TEM samples were electrolytically thinned in a solution consisting of 95 parts methanol and 5 parts sulphuric acid, cooled to approximately 220 K. The hardness and strength of the specimens were measured using a Vickers microhardness tester with a 100 g load and an Instron-type tensile testing machine at a strain rate of $1.7 \times 10^{-4}\,\mathrm{sec}^{-1}$. The crystallization temperature of the alloys was examined at a heating rate of $8.3 \times 10^{-2}\,\mathrm{K\,sec}^{-1}$ in a differential thermal analyser (DTA). The ductile–brittle transition behaviour was tested for the specimens annealed for 1 h at various temperatures in evacuated quartz tubes. Ductility was evaluated by measuring the radius of curvature at fracture in a simple bend test [16].

The superconducting transition was monitored by measuring the electrical resistivity of the alloys in the amorphous as well as annealed state by a conventional four-probe method. The specimen current used was 1 mA. The temperature was measured using a calibrated Au–Fe + Chromel thermocouple with an accuracy of ± 0.05 K. The critical current was defined as the current at which a measurable voltage (1 μV) appeared across a 50 mm length of the specimen in a liquid helium bath at no applied field. The critical magnetic field (H_c) measurement was performed using a superconducting solenoid for magnetic fields up to about $7.2 \times 10^6\,\mathrm{A\,m}^{-1}$ applied transversely to the specimen in a liquid helium bath.

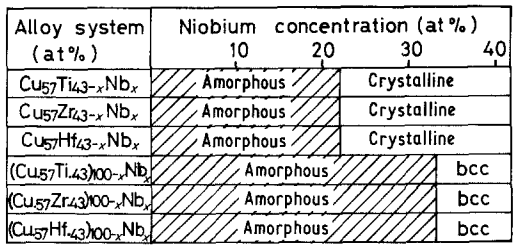

Figure 1 Composition ranges for the formation of an amorphous phase in the Cu–Nb–Ti, Cu–Nb–Zr and Cu–Nb–Hf systems.

3. Results

3.1. Formation range of amorphous phase

Fig. 1 shows the composition range in which the amorphous phase was found to form without any trace of crystallinity in the Cu–Nb–Ti, Cu–Nb–Zr and Cu–Nb–Hf ternary systems. The amorphous phase forms in the wide range of 0 to 22 at% Nb for $Cu_{57}M_{43-x}Nb_x$ (M = Ti, Zr, Hf) alloys and 0 to 33 at% Nb for $(Cu_{0.57}M_{0.43})_{100-x}Nb_x$ alloys. The formation range is much wider for the alloys with the ratio of M/Cu being equal to 43/57 (M = Ti, Zr, Hf) which appears to be most appropriate for the formation of the amorphous phase [17]. This indicates that the interaction between Cu and M atoms plays a significant role in the formation of the amorphous phase in metal–metal systems. Further, one can see in Fig. 1 that a b c c phase appears in the $(Cu_{0.57}M_{0.43})_{100-x}Nb_x$ alloys containing more than 33 at% Nb. As examples, typical electron micrographs of the amorphous and the b c c phase in the thinned $Cu_{40}Nb_{30}Zr_{30}$ and $Cu_{34}Nb_{40}Zr_{26}$ alloys are shown in Fig. 2, together with the selected area diffraction patterns. Lack of contrast in the bright-field image of Fig. 2a and the presence of diffuse haloes in the diffraction pattern of Fig. 2b clearly indicate that the melt-quenched $Cu_{40}Nb_{30}Zr_{30}$ alloy is amorphous. No

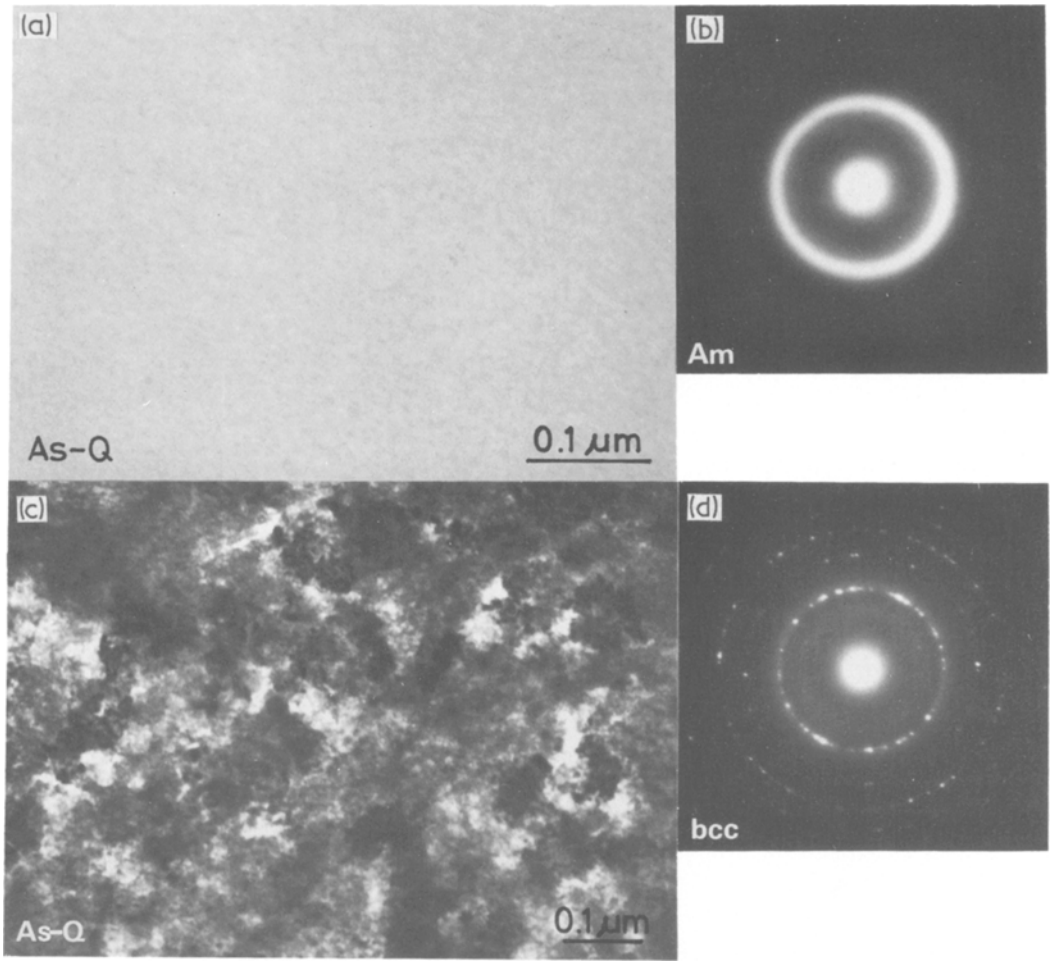

Figure 2 Transmission electron micrographs and selected area diffraction patterns showing the as-quenched structures of (a) and (b) $Cu_{40}Nb_{30}Zr_{30}$ and (c) and (d) $Cu_{34}Nb_{40}Zr_{26}$ alloys.

evidence of crystalline inclusions was found by means of dark-field electron microscopy for all the alloys within the amorphous-forming ranges described above. Dark contrast in the bright-field image of Fig. 2c and the ring spots in the diffraction pattern of Fig. 2d indicate that the melt-quenched $Cu_{34}Nb_{40}Zr_{26}$ alloy contains a large number of internal defects and the size of grain and/or sub-grain is small. It is also to be noticed that even the alloys with such a b c c structure exhibit a good luster and are so ductile that no crack is found at the tip of a specimen bent through 180°, similar to other amorphous alloys. Both X-ray and electron diffraction analyses indicate that the as-quenched $Cu_{34}Nb_{40}Zr_{26}$ alloys consist of a phase with a b c c structure with $a \simeq 0.330$ nm. This value is close to the lattice parameter ($a = 0.3301$ nm) of niobium [18], suggesting that the b c c phase may be a niobium-rich supersaturated solid solution containing a large amount of copper and/or zirconium.

3.2. Mechanical properties and crystallization temperature

Vickers hardness (H_v), tensile fracture strength (σ_f), crystallization temperature (T_x), critical fracture temperature (T_f) and the ratio T_f/T_x of $Cu_{40}Nb_{30}M_{30}$ (M = Ti, Zr, Hf) amorphous alloys are presented in Table I, wherein T_f is the temperature of ageing for 1 h which led to the fracture of alloys in a simple bend test. The hardness values and the tensile strengths are in the range 440 to 510 diamond pyramid number (DPN) and 1600 to 1800 MPa, respectively. The crystallization temperatures of these alloys are in the range 740 to 835 K. As seen in Table I, there is no

TABLE I Vickers hardness (H_v), tensile fracture strength (σ_f), crystallization temperature (T_x), critical fracture temperature (T_f) and T_f/T_x for $Cu_{40}Nb_{30}M_{30}$ (M = Ti, Zr and Hf) amorphous alloys

Alloy system (at %)	Vickers hardness, H_v (DPN)	Fracture strength, σ_f (MPa)	Crystallization temperature, T_x (K)	Critical fracture temperature, T_f (K)	T_f/T_x
$Cu_{40}Nb_{30}Ti_{30}$	510	1800	808	625	0.77
$Cu_{40}Nb_{30}Zr_{30}$	440	1600	739	700	0.95
$Cu_{40}Nb_{30}Hf_{30}$	460	1600	833	750	0.90

systematic change in H_v, σ_f or T_x by the replacement of Ti, Zr or Hf.

Furthermore, these amorphous alloys possess good bend ductility. That is, when these specimens were completely bent by pressing against the edge of a razor blade, numerous deformation markings were seen near the bent edge, but no cracks were observed even with such severe deformation. Tensile fracture occurred on the shear plane at about 50° to the tensile axis in the direction of thickness and the fracture surface consisted of a smooth part produced by shear slip and a vein-like part produced by plastic instability, in a way similar to the fracture morphology of other metal–metal amorphous alloys such as Cu-Zr [17], Co–Ti [19], (Fe, Co Ni)–Zr [20, 21] and (Fe, Co, Ni)–Hf [22, 23].

Ductile–brittle transition behaviour for $Cu_{40}Nb_{30}Ti_{30}$, $Cu_{40}Nb_{30}Zr_{30}$ and $Cu_{40}Nb_{30}Hf_{30}$ amorphous alloys was examined as a function of ageing time and temperature. As an example, their embrittlement behaviour during isochronal ageing for 1 h is shown in Fig. 3, in which the results of $Cu_{57}Hf_{43}$ amorphous alloys found in the present work is also represented for comparison. The strain on the outer surface required for fracture, ϵ_f, is estimated from the relation $\epsilon_f = t/(2r - t)$, where r is the radius of curvature of the bent sample at fracture and t is the thickness of the ribbon specimen. The temperatures (T_f) where the fracture starts and the values of T_f/T_x are about 625 K and 0.77 for $Cu_{40}Nb_{30}Ti_{30}$, about 700 K and 0.95 for $Cu_{40}Nb_{30}Zr_{30}$ and about 750 K and 0.90 for $Cu_{40}Nb_{30}Hf_{30}$. Thus, the embrittlement tendency of the metal–metal amorphous alloys on ageing differs considerably among $Cu_{40}Nb_{30}M_{30}$ (M = Ti, Zr, Hf) alloys and the amorphous alloys containing zirconium or hafnium are less susceptible to embrittlement than the titanium-containing alloys. This embrittlement tendency agrees well with the previous result that (Fe, Co, Ni)–Zr [21] and (Fe, Co, Ni)–Hf [23] binary amorphous alloys are less susceptible to embrittlement than the Co–Ti [19] binary alloy, suggesting the tendency that the larger the period number of the solute element, the lower is the embrittlement tendency of the alloy. Such a tendency also receives support from the fact that the addition of niobium does not result in any loss of thermal embrittlement of the Cu–Hf amorphous alloy, as seen in Fig. 3.

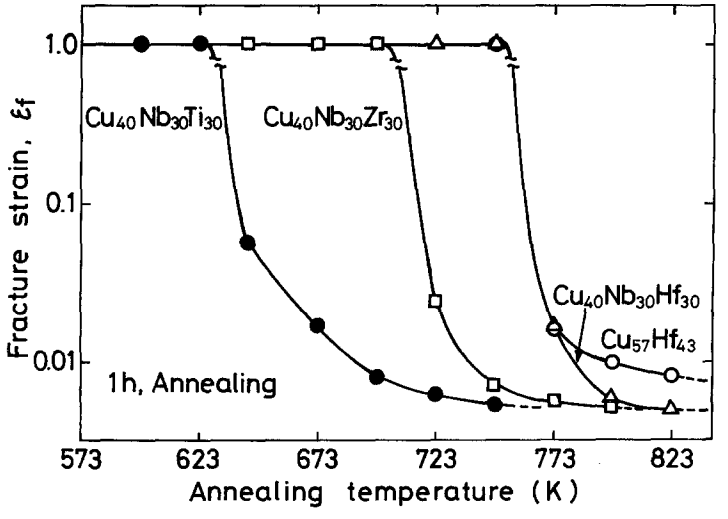

Figure 3 Change in fracture strain of $Cu_{40}Nb_{30}M_{30}$ (M = Ti, Zr, Hf) amorphous alloys after annealing for 1 h at various temperatures. The result of $Cu_{57}Hf_{43}$ amorphous alloy is also included for comparison.

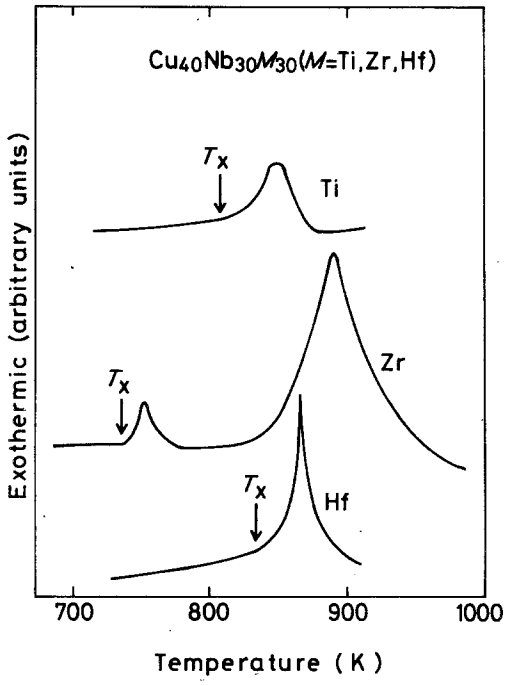

Figure 4 Differential thermal analysis curves of $Cu_{40}Nb_{30}Ti_{30}$, $Cu_{40}Nb_{30}Zr_{30}$ and $Cu_{40}Nb_{30}Hf_{30}$ amorphous alloys.

3.3. Crystallization behaviour

Fig. 4 shows the DTA curves of the $Cu_{40}Nb_{30}M_{30}$ (M = Ti, Zr, Hf) alloys. The $Cu_{40}Nb_{30}Zr_{30}$ alloy exhibits two clear exothermic peaks starting at 739 and 823 K, while the $Cu_{40}Nb_{30}Ti_{30}$ and $Cu_{40}Nb_{30}Hf_{30}$ alloys show a single peak each at 808 and 833 K, respectively. This is an unexpected result because titanium, zirconium and hafnium belong to the same group in the periodic table and a similar behaviour was anticipated.

The amorphous alloys were heat treated at the crystallization temperatures for 10 min, 30 min and 1 h with a view to following the crystallization behaviour of the amorphous alloy and also to correlating the microstructure with the superconducting properties.

Fig. 5a and b show the microstructure and the corresponding diffraction pattern of a $Cu_{40}Nb_{30}Ti_{30}$ alloy annealed for 30 min at 808 K. The diffraction pattern clearly indicates that some type of ordering has taken place. Longer annealing treatments at the same temperature (e.g. 1 h) resulted in a better development of the order, as indicated by Fig. 5c. In the case of the

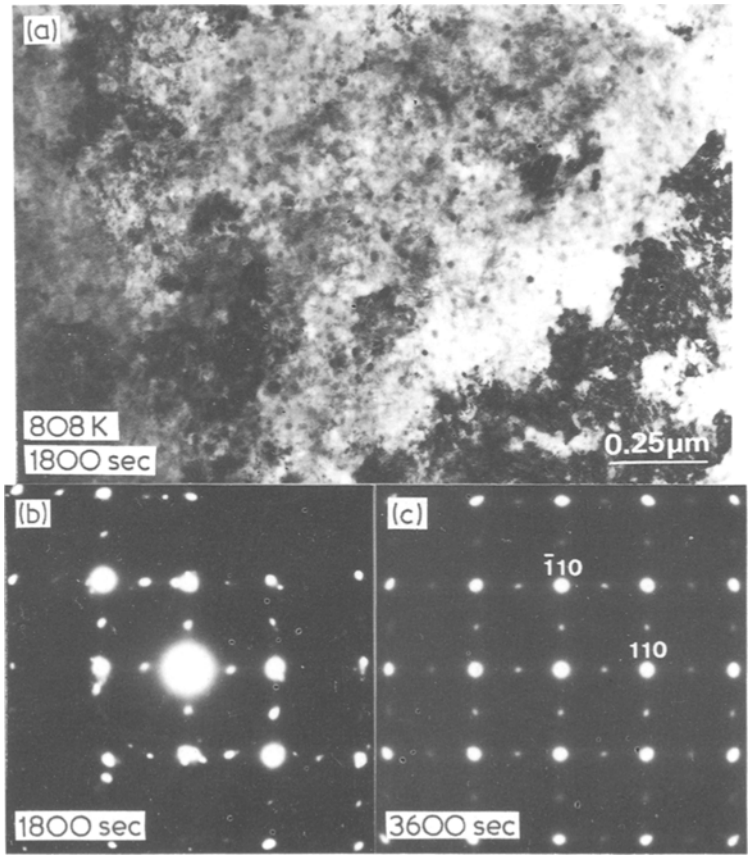

Figure 5 Transmission electron micrograph and selected area diffraction patterns of $Cu_{40}Nb_{30}Ti_{30}$ amorphous alloy annealed (a) and (b) at 808 K for 0.5 h and (c) for 1 h.

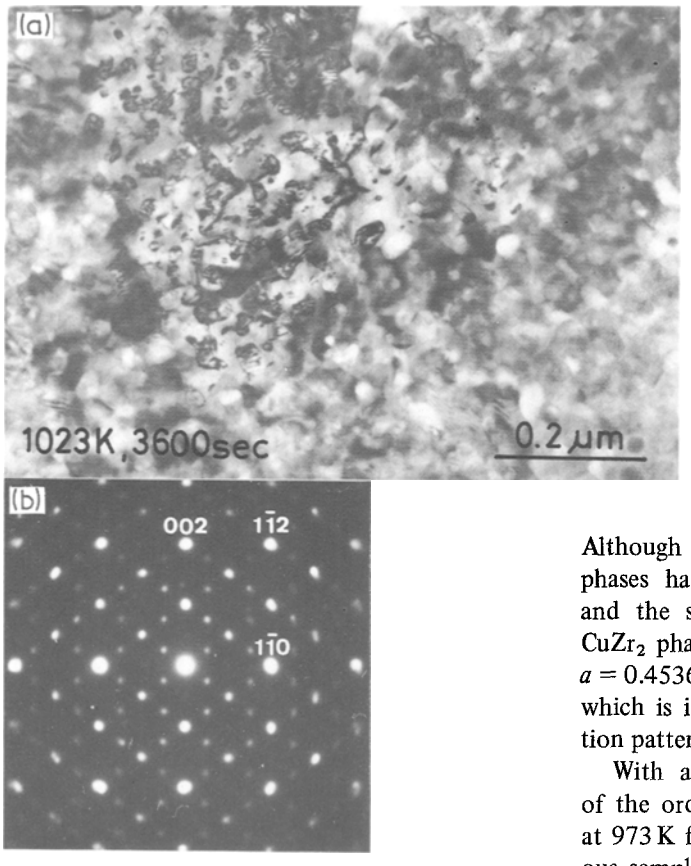

Figure 6 (a) Transmission electron micrograph and (b) selected area diffraction pattern of $Cu_{40}Nb_{30}Hf_{30}$ amorphous alloy annealed at 1023 K for 1 h.

$Cu_{40}Nb_{30}Hf_{30}$ alloy, also when heat treated for 1 h at 1023 K, ordering is clearly noticed, as can be seen in Fig. 6. In the case of $Cu_{40}Nb_{30}Zr_{30}$, however, it was not possible to detect the presence of any ordered phases, as seen in Fig. 7.

The ordered phases shown in Fig. 5 can be described as being based on a b c c unit cell with a lattice parameter a of about 0.31 nm. The ordering, however, appears to result in a complex structure. For example, Fig. 5c can be indexed as the [0 0 1] orientation of the b c c reciprocal lattice. The ordered reflections can be seen at positions corresponding to $\{\frac{1}{2}\frac{1}{2}0\}$. Surprisingly, spots at {1 0 0} and related positions are absent. This might indicate that ordering may be complex due to preferential occupation of the constituent atoms leading to extinction conditions for the {1 0 0}-type reflections.

None of the equilibrium phases of the constituent binary diagrams of the above systems show any ordered structures [24]. Thus, these may be considered as metastable. Binary Cu–Zr alloys feature several complex intermediate phases. Although the stoichiometry of some of these phases has been determined, the crystal system and the structure are still uncertain [25]. The $CuZr_2$ phase possessing a tetragonal structure with $a = 0.4536$ and $c = 0.3716$ nm [26] is one phase which is identified unambiguously in our diffraction patterns.

With a view to confirming the metastability of the ordered phases, long annealing treatments at 973 K for 24 h have been given to the amorphous samples. Fig. 8a and b show a typical bright-field micrograph and the corresponding diffraction pattern for the $Cu_{40}Nb_{30}Ti_{30}$ heat treated under the above conditions. The diffraction pattern can be satisfactorily indexed on the basis of the equilibrium Cu_4Ti_3-phase (tetragonal, $a = 0.313$ nm and $c = 1.994$ nm) [27]. The structure of this phase can be derived if one visualizes stacking of 7 b c c unit cells with $a \simeq 0.31$ nm in the c-direction and proposing a slight compression in the c-direction. This will result in

$$a_{\text{tetr.}} \simeq a_{\text{bcc}} \quad \text{and} \quad c_{\text{tetr.}} \simeq 7 \times a_{\text{bcc}}.$$

As can be seen in the diffraction pattern of Fig. 8b, the distance between two intense spots in the [0 0 2] direction is subdivided into seven parts. Such a periodicity of 7 is observed in several other diffraction patterns also. It is worth recalling in this context that the ordered phases are also based on a b c c unit cell with $a \simeq 0.31$ nm. Thus, the decomposition behaviour of the amorphous phase may be visualized as follows

$$\text{Amorphous} \rightarrow \text{b c c} \rightarrow \text{ordered structure} \rightarrow \text{equilibrium phases}.$$

The above sequence is followed quite closely in

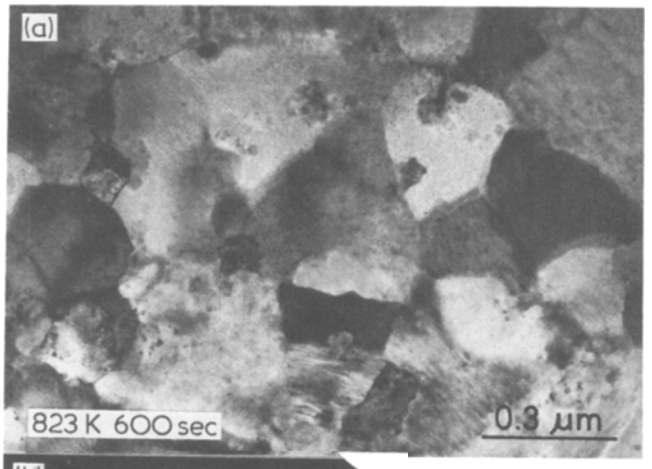

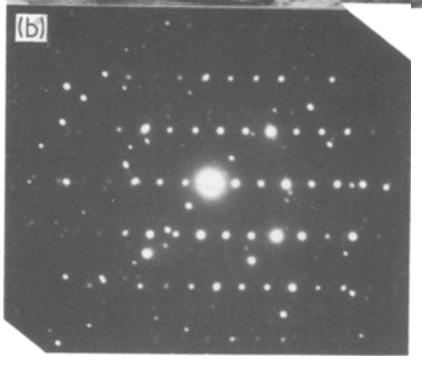

Figure 7 (a) Transmission electron micrograph and (b) selected area diffraction pattern of $Cu_{40}Nb_{30}Zr_{30}$ alloy annealed at 823 K for 10 min.

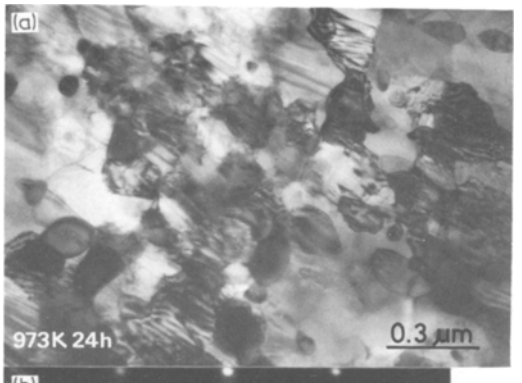

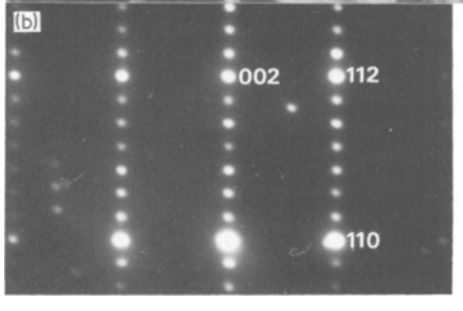

Figure 8 (a) Transmission electron micrograph and (b) selected area diffraction pattern of $Cu_{40}Nb_{30}Ti_{30}$ alloy annealed at 973 K for 24 h.

the $Cu_{40}Nb_{30}Ti_{30}$ and $Cu_{40}Nb_{30}Hf_{30}$ alloys. However, the equilibrium phases precipitate directly from the amorphous phase in the $Cu_{40}Nb_{30}Zr_{30}$ alloy.

3.4. Superconducting properties

Figs 9 and 10 show the reduced electrical resistance curves in the vicinity of T_c for the $Cu_{40}Nb_{30}Ti_{30}$ and $Cu_{40}Nb_{30}Hf_{30}$ amorphous alloys in the as-quenched as well as 1 h annealed states in the case of no applied magnetic field. Also, the T_c and ΔT_c values of their amorphous alloys are plotted in Fig. 11 as a function of the annealing temperature. The value of T_c is taken as the temperature at which the resistance ratio, $R/R_n = 0.5$, where R_n is the resistance in the normal state. The transition width ΔT_c, represented by the vertical bar, corresponds to the temperature difference between 0.1 and $0.9\,R/R_n$. As seen in these figures, the amorphous specimens remain in a normal state down to the temperature of liquid helium (4.2 K). Annealing at temperatures above 823 K for $Cu_{40}Nb_{30}Ti_{30}$ and above 973 K for $Cu_{40}Nb_{30}Hf_{30}$ results in a transition to the superconducting state above the liquid helium temperature. For the two specimens, T_c increases with increasing annealing temperature, shows maximum values at appropriate temperatures and decreases with further annealing. The highest T_c values attained are 5.6 K for $Cu_{40}Nb_{30}Ti_{30}$ and 8.4 K for $Cu_{40}Nb_{30}Hf_{30}$. Further, one can see that the annealing temperatures giving rise to the maximum T_c are quite different for the two alloys, despite the fact that the difference in crystallization temperatures is as small as 25 K. Although the reason for such a large difference is uncertain at present, it may be due to the fact [28] that the melting

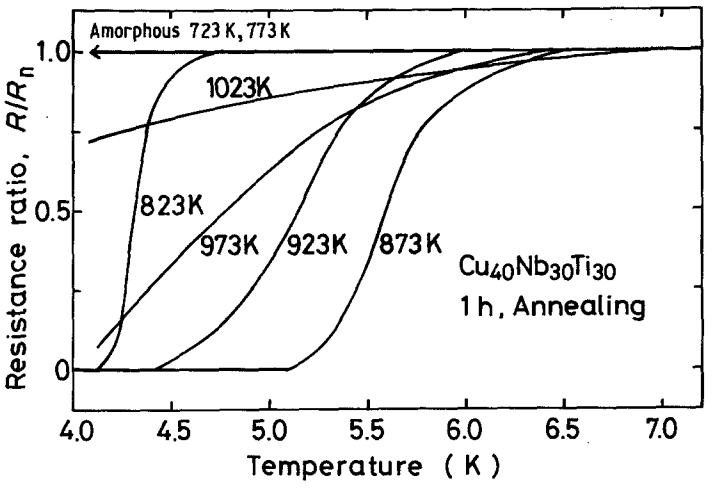

Figure 9 Resistance ratio R/R_n as a function of temperature for $Cu_{40}Nb_{30}Ti_{30}$ amorphous alloy annealed for 1 h at various temperatures.

and boiling points (2495 and 5673 K) of hafnium are much higher than those (1941 and 3533 K) of titanium. The ΔT_c of specimens possessing the maximum T_c is about 0.6 K, but with decreasing or increasing annealing temperature it shows a tendency to increase. Surprisingly, $Cu_{40}Nb_{30}Zr_{30}$ did not exhibit superconductivity on annealing at any temperature in the range 773 to 1173 K despite the homologous alloy composition. Detailed discussion on this point will be given in the next section based on the difference in annealed structure.

The upper critical magnetic field, H_{c2}, was measured at liquid helium temperature using a standard four-probe resistance method. The H_{c2} (onset) values obtained were $1.8 \times 10^6 A m^{-1}$ for $Cu_{40}Nb_{30}Ti_{30}$ and $2.3 \times 10^6 A m^{-1}$ for $Cu_{40}Nb_{30}Hf_{30}$, following a general tendency [29] that the higher the T_c, the higher is H_{c2}.

Further, the critical current density, J_c, was measured with an external applied magnetic field (H) in a liquid helium bath. As an example, Fig. 12 shows the critical current density $J_c(H)$ as a function of H for the $Cu_{40}Nb_{30}Hf_{30}$ alloy annealed for 1 h at 1073 K, where T_c shows the maximum value. For $H = 0$, J_c is found to be about $1 \times 10^4 A cm^{-2}$. For $H > 0$, J_c is observed to fall rapidly with increasing H. For example, at $H \simeq 0.5 H_{c2}$, J_c is of the order of $700 A cm^{-2}$. Such small values of J_c at external applied magnetic field (H) indicate that flux pinning forces in this material are comparatively weak.

4. Discussion

The structure on annealing and the superconducting properties of $Cu_{40}Nb_{30}M_{30}$ (M = Ti, Zr and Hf) alloys crystallized at temperatures where T_c shows a maximum value are summarized in Table

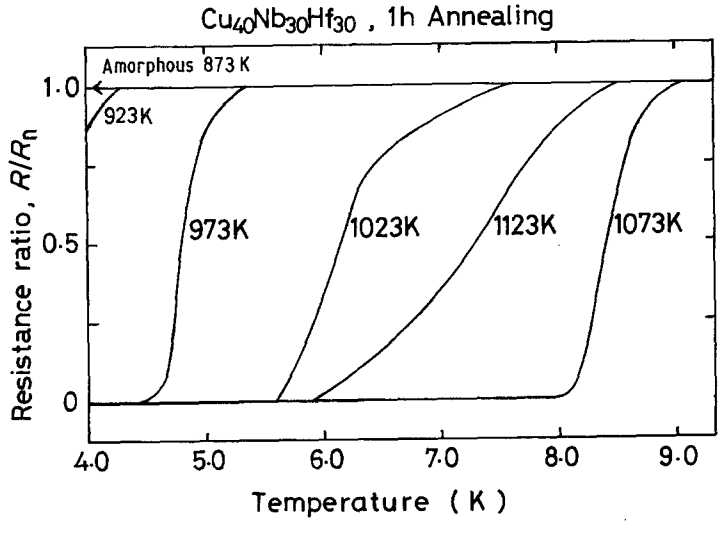

Figure 10 Resistance ratio R/R_n as a function of temperature for $Cu_{40}Nb_{30}Hf_{30}$ amorphous alloy annealed for 1 h at various temperatures.

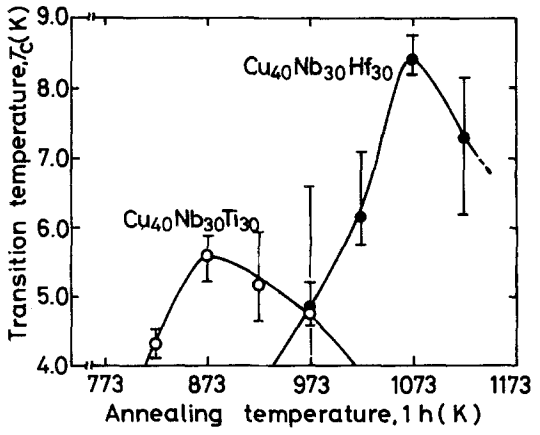

Figure 11 Change of superconducting transition temperature T_c for $Cu_{40}Nb_{30}Ti_{30}$ and $Cu_{40}Nb_{30}Hf_{30}$ amorphous alloys with annealing temperature. The vertical bars correspond to ΔT_c.

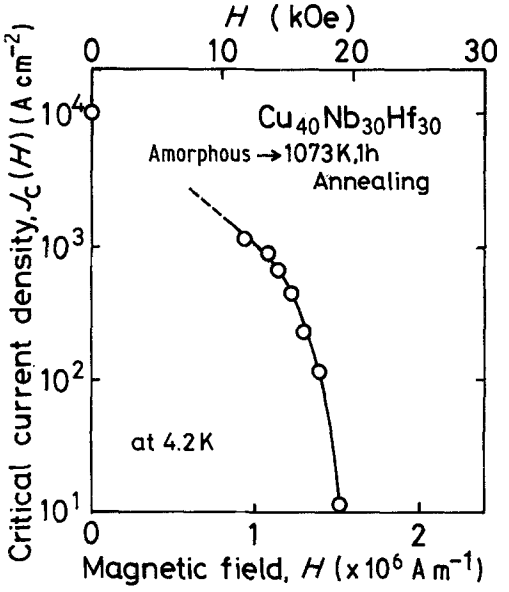

Figure 12 Critical current density $J_c(H)$ of $Cu_{40}Nb_{30}Hf_{30}$ amorphous alloy annealed for 1 h at 1073 K as a function of magnetic field applied normal to the direction of current flow.

II. As shown in this table and Fig. 11, the superconductivity at temperatures above 4.0 K appears in the range 820 to 1020 K for $Cu_{40}Nb_{30}Ti_{30}$ and above 950 K for $Cu_{40}Nb_{30}Hf_{30}$ and their superconducting alloys consist of ordered phases based on a b c c lattice with a lattice parameter a of 0.31 nm. On the other hand, the $Cu_{40}Nb_{30}Zr_{30}$ alloy does not show superconductivity in any annealed condition and no ordered phase was found. Judging from the fact that the temperature range where superconductivity appears agrees well with that of the precipitation of the ordered b c c phase, it is reasonably concluded that the superconductivity for the $Cu_{40}Nb_{30}Ti_{30}$ and $Cu_{40}Nb_{30}Hf_{30}$ alloys is due to the precipitation of the metastable ordered b c c phases. Further, these alloys appear to be Type-II superconductors since H_{c2} possesses relatively large values.

Although the reason why the metastable superconducting phase with the ordered b c c structure appears only in Cu–Nb–Ti and Cu–Nb–Hf alloys and some non-superconducting complex compounds appear directly in the Cu–Nb–Zr alloy is uncertain at present, it may be due to a difference in atomic size among the constituent elements in the amorphous alloys. Since atomic size decreases in the order zirconium > hafnium > titanium > niobium > copper [30], the b c c solid solution is formed in the alloys containing titanium or hafnium which possess a smaller difference in atomic size compared with niobium or copper, whereas complex compounds appear instead of the solid solution in the alloy containing zirconium which possesses a much larger atomic size than niobium or copper. That is, it may be said that the atomic size of zirconium is too large to form the b c c solid solution. It is hoped that systematic investigations [31], currently in progress, on the annealed structure and superconducting properties of $Cu_{40}V_{30}M_{30}$ and $Cu_{40}Ta_{30}M_{30}$ (M = Ti,

TABLE II Annealing structure transition temperature (T_c), transition width (ΔT_c), critical current density (J_c) and upper critical magnetic field (H_{c_2}) for $Cu_{40}Nb_{30}M_{30}$ (M = Ti, Zr and Hf) amorphous alloys

Alloy system (at %)	Annealing structure	T_c (K)	ΔT_c (K)	J_c (A cm^{-2})	H_{c_2} (A m^{-1})
$Cu_{40}Nb_{30}Ti_{30}$	Ordered b c c (873 K, 1 h)	5.6	0.7	2×10^3	1.8×10^6
$Cu_{40}Nb_{30}Hf_{30}$	Ordered b c c (1073 K, 1 h)	8.5	0.6	1×10^4	2.3×10^6
$Cu_{40}Nb_{30}Zr_{30}$	b c c + $CuZr_2$ + compound (973 K, 1 h)	Non-superconducting down to 4.0 K			

Zr, Hf) amorphous alloys will shed some light on this problem.

5. Conclusions

New metal–metal types of amorphous alloys exhibiting high strength and good bend ductility were found in the Cu–Nb–(Ti, Zr, Hf) ternary systems. Specimens were produced in the form of continuous ribbons of about 1 to 2 mm width and about 0.02 to 0.03 mm thickness using a conventional melt spinning apparatus adapted to an induction furnace. The amorphous alloys could be produced up to a niobium content of 35 at% and the titanium, zirconium or hafnium content was between 25 and 50 at%. Vickers hardness and tensile strength were about 440 to 510 DPN and 1600 to 1800 MPa, respectively. Crystallization temperatures were in the range 740 to 835 K. Further, these amorphous alloys were so ductile that no crack was found at the tip of a specimen bent through 180°. The ductility remained unchanged for 1 h at temperatures below 625 K for $Cu_{40}Nb_{30}Ti_{30}$, 700 K for $Cu_{40}Nb_{30}Zr_{30}$ and 750 K for $Cu_{40}Nb_{30}Hf_{30}$. In addition, the $Cu_{40}Nb_{30}Ti_{30}$ and $Cu_{40}Nb_{30}Hf_{30}$ alloys showed a superconducting transition above the liquid helium temperature (4.2 K) after crystallizing at temperatures above 823 and 923 K respectively and the structures consisted of ordered phases based on a b c c lattice with a lattice parameter a of 0.31 nm. The transition temperature T_c increased with increasing annealing temperature, showed maximum values at appropriate temperatures and decreased with further annealing. The highest T_c values attained were 5.6 K for $Cu_{40}Nb_{30}Ti_{30}$ and 8.4 K for $Cu_{40}Nb_{30}Hf_{30}$. The same variation with annealing temperature was recognized for the upper critical magnetic field H_{c2} and the critical current density J_c. The values obtained of H_{c2} at 4.2 K and J_c at zero applied field and 4.2 K were of the order of 1.8×10^6 A m^{-1} and 2×10^3 A cm^{-2} for $Cu_{40}Nb_{30}Ti_{30}$ and 2.3×10^6 A m^{-1} and 1×10^4 A cm^{-2} for $Cu_{40}Nb_{30}Hf_{30}$. On the other hand, $Cu_{40}Nb_{30}Zr_{30}$ did not exhibit superconductivity even in the annealed condition and no ordered phase was found. From the fact that the temperature range where superconductivity appeared agreed well with that of the precipitation of the ordered b c c phase, it was reasonably concluded that the superconductivity in the $Cu_{40}Nb_{30}(Ti, Hf)_{30}$ alloys resulted from the precipitation of the metastable ordered b c c phases.

Acknowledgements

The authors are indebted to Mr. A. Hoshi of the High Magnetic Field Laboratory of Tohoku University for critical magnetic field measurements. One of the authors (CS) would like to thank the Japan Society for the Promotion of Science for financial assistance.

References

1. W. L. JOHNSON, "Rapidly Quenched Metals III", Vol. 2 edited by B. Cantor, (The Metals Society, London, 1978) p. 1.
2. W. L. JOHNSON, *J. Appl. Phys.* **50** (1979) 1557.
3. A. INOUE and T. MASUMOTO, "Structure and Properties of Amorphous Metals II", edited by T. Masumoto and T. Imura, Supplement to *Sci. Rep. Res. Inst. Tohoku University* **A28** (1980) 165.
4. T. MASUMOTO, A. INOUE, S. SAKAI, H. M. KIMURA and A. HOSHI, *Trans. Jap. Inst. Met.* **21** (1980) 115.
5. A. INOUE, S. SAKAI, H. M. KIMURA, T. MASUMOTO and A. HOSHI, *Scripta Met.* **14** (1980) 235.
6. A. INOUE, C. SURYANARAYANA, T. MASUMOTO and A. HOSHI, *Sci. Rep. Res. Inst. Tohoku University* **A28** (1980) 182.
7. T. MASUMOTO and A. INOUE, Paper to Workshop on High Field Superconducting Materials for Fusion in US–Japan Co-operation Programme, Tokyo, March, 1980.
8. A. INOUE, C. SURYANARAYANA, T. MASUMOTO and A. HOSHI, *Mater. Sci. Eng.* **47** (1981) 69.
9. A. INOUE, H. M. KIMURA, T. MASUMOTO, C. SURYANARAYANA and A. HOSHI, *J. Appl. Phys.* **51** (1980) 5475.
10. A. INOUE, T. MATSUMOTO, C. SURYANARAYANA and A. HOSHI, *J. de Phys. 41 Colloque* **C-8** (1980) 758.
11. C. SURYANARAYANA, A. INOUE and T. MASUMOTO, *Scripta Met.* **14** (1980) 881.
12. A. INOUE, A. HOSHI, C. SURYANARAYANA and T. MASUMOTO, *ibid.* **14** (1980) 1077.
13. A. INOUE, T. MASUMOTO, A. HOSHI and S. SAKAI, International Conference on Metallic Glasses, Science and Technology, Budapest, June/July, 1980.
14. A. INOUE, S. SAKAI, H. M. KIMURA and T. MASUMOTO, *Trans. Jap. Inst. Met.* **20** (1979) 255.
15. A. INOUE, H. M. KIMURA, S. SAKAI and T. MASUMOTO, Fourth International Conference on Titanium, Kyoto, Japan, May, 1980.
16. A. INOUE, T. MASUMOTO and H. M. KIMURA, *J. Jap. Inst. Met.* **42** (1978) 303; *Sci. Rep. Res. Inst. Tohoku University* **A27** (1979) 159.
17. R. RAY, B. C. GIESSEN and N. J. GRANT, *Scripta Met.* **2** (1968) 357.
18. W. B. PEARSON, "A Handbook of Lattice Spacings and Structures of Metals and Alloys" (Pergamon Press, Oxford, 1967) p. 769.
19. A. INOUE, K. KOBAYASHI, C. SURYANA-

RAYANA and T. MASUMOTO, *Scripta Met.* **14** (1980) 119.
20. K. H. J. BUSCHOW and N. M. BEEKMANS, *Phys. Rev. B* **19** (1979) 3843.
21. M. NOSE and T. MASUMOTO, *Sci. Rep. Res. Inst. Tohoku University* **A28** (1980) 332.
22. K. H. J. BUSCHOW and N. M. BEEKMANS, *J. Appl. Phys.* **50** (1979) 6348.
23. A. INOUE, K. KOBAYASHI and T. MASUMOTO, International Conference on Metallic Glasses, Science and Technology, Budapest, June/July, 1980.
24. Metals Handbook, eight edition, "Metallography, Structures and Phase Diagrams" (American Society for Metals, Metals Park, Ohio, 1973) p. 302 and 359.
25. Metals Handbook, eigth edition, "Metallography, Structures and Phase Diagrams" (American Society for Metals, Metals Park, Ohio, 1973) pp. 281, 282, 284, 285, 300 and 302.
26. W. B. PEARSON, "A Handbook of Lattice Spacings and Structures of Metals and Alloys" (Pergamon Press, Oxford, 1967) p. 623.
27. K. SCHUBERT, *Z. Metallkde* **56** (1965) 197.
28. Metals Databook, (The Japanese Institute of Metals, Maruzen, Japan, 1974) p. 10.
29. G. EILENBERGER and V. AMBEGAOKAR, *Phys. Rev.* **158** (1967) 332.
30. Metals Databook, (The Japanese Institute of Metals, Maruzen, Japan, 1974) p. 8.
31. A. INOUE, Y. TAKAHASHI and T. MASUMOTO, unpublished work (1981).

Received 28 July and accepted 4 September 1980.